The Holocene 13,3 (2003) pp. 353–363

Holocene glacier variability: three case studies using an intermediate-complexity climate model

S.L. Weber[1]* and J. Oerlemans[2]

([1]Royal Netherlands Meteorological Institute (KNMI), PO Box 201, 3730 AE De Bilt, The Netherlands; [2]Institute for Marine and Atmospheric Research, Utrecht University, Princetonplein 5, 3584 CC Utrecht, The Netherlands)

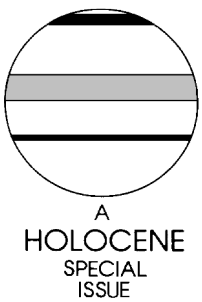

Abstract: Synthetic glacier length records are generated for the Holocene epoch using a process-based glacier model coupled to the intermediate-complexity climate model ECBilt. The glacier model consists of a mass-balance component and an ice-flow component. The climate model is forced by the insolation change due to variations in the Earth's orbital parameters. We consider three glaciers, ranging from maritime to continental. At Nigardsbreen (southern Norway), the simulated long-term trend in the annual mass-balance is primarily determined by summer temperature, with a smaller contribution from winter precipitation. In the early Holocene, summers were warmer and winters wetter than today in the ECBilt simulation. Both signals seem consistent with proxy data. The simulated glacier length shows a phase of rapid expansion during the mid-Holocene, followed by more gradual growth. At Rhonegletscher (the Swiss Alps), ECBilt simulates warmer and wetter summers in the early Holocene. The temperature signal seems realistic, but proxy data and earlier modelling results are not conclusive with respect to the precipitation signal. The implied glacier length shows a maximum extent at 3–5 kyr BP, which seems unlikely. This suggests that the simulated precipitation response is not realistic. The simulated early-Holocene climate at Abramov glacier (Kirghizia) is characterized by high summer precipitation, associated with a northward extension of the Asian monsoon. The precipitation signal reaches its maximum around 6 kyr BP, which is consistent with the timing of the maximum in lake-level data. The simulated glacier length shows a pronounced postglacial maximum at the time of maximum monsoon intensity. There is considerable centennial-timescale variability in the simulated glacier length records. These length variations are generated by internal climatic variability. They are typically asynchronous among the three different glaciers. ECBilt has reasonable skill in simulating the relative importance of temperature and precipitation as well as the seasonality of the forcing, although the overall level of variability is underestimated. Length variations are shown to behave as a lagged moving-average process, with a glacier-specific memory.

Key words: Glacier variations, mass balance, climate forcing, intermediate-complexity modelling, glacier model, climate model, glacier length, precipitation, monsoon, Holocene.

Introduction

Glacier fluctuations are an impressive manifestation of varying climatic conditions. A well-known example is the extensive glacial advances in western Europe during the period known as the 'Little Ice Age'. To reconstruct past climatic conditions from observed glacier fluctuations in an unambiguous manner is, however, difficult. There are several reasons for this. First, the glacier mass-balance is sensitive to a number of atmospheric parameters (mainly temperature and precipitation) and the sensitivity depends on the time of the year. For example, high winter precipitation and low summer temperatures have a similar effect on the glacier mass-balance. Second, glacier length responds with a delay to the integrated mass-balance variations. This becomes clear when the overall glacier geometry is considered. There is accumulation at the higher part of the glacier and ablation at the lower part. Integrated over the total glacier surface, this gives the net mass-balance. A non-zero mass-balance will result in anomalous downward ice flow. Because of the long timescale of this process, only persistent mass-balance anomalies are effective. These result in a delayed response of the glacier snout. Third, all glaciers have their own specific mass-balance sensitivity and response time.

Clearly, it is crucial to develop process-based glacier models in order to be able to interpret past glacier fluctuations. Such models construct glacier length from the meteorological forcing conditions, given the glacier characteristics. In the present paper, a process-based glacier model is used to generate synthetic glacier length records. The glacier model consists of a mass-balance model and a dynamic ice-flow model. The climate forcing is generated by a global General Circulation Model (GCM). Such

*Author for correspondence (e-mail: weber@knmi.nl)

10.1191/0959683603hl628rp

an approach was used earlier by Reichert *et al.* (2002). They examined glacier fluctuations forced by internal variability of the climatic system, using multicentury GCM simulations.

The intermediate-complexity climate model ECBilt (Opsteegh *et al.*, 1998) was used in the present experiment. It is a coupled atmosphere/ocean/sea-ice model containing simplified parameterizations of the subgrid-scale physical processes. ECBilt is computationally more efficient than a comprehensive GCM like, for example, the ECHAM climate model used by Reichert *et al.* (2002). Therefore, it is possible to perform very long simulations.

The present paper examines glacier fluctuations throughout the Holocene epoch, taking orbital forcing into account. Other external forcings, like solar irradiance changes, volcanic eruptions or anthropogenic effects, are excluded. The simulated glacier length records are analysed with respect to long-term changes related to the orbital forcing as well as variability on shorter timescales. We consider three glaciers: Nigardsbreen, Rhonegletscher and Abramov glacier. Nigardsbreen (62°N, 7°E) is a maritime glacier, situated in southern Norway. Rhonegletscher (47°N, 8°E), located at high altitudes in the Swiss Alps, has a more continental character. Abramov glacier (40°N, 72°E) is in the republic of Kirghizia, north of Pakistan, which has a pure continental climate.

The models

The climate model

ECBilt (Opsteegh *et al.*, 1998) is a global climate model of intermediate complexity. It was primarily designed to study atmosphere-ocean dynamics in the mid-latitudes and the associated variability on timescales ranging from days to millennia. The atmospheric component is a moist dynamic model, which resolves synoptic-scale variability. It incorporates simplified representations of the diabatic-heating processes and the hydrological cycle. There is a land-surface parameterization, based on a bucket model for soil moisture and a thermodynamic snow model. The horizontal resolution is about 500 km in mid-latitudes (spectral T21). The atmospheric component is computationally efficient, due to its coarse vertical resolution (three levels) and simplified parameterization package. It is synchronously coupled to a dynamic ocean model and a thermodynamic sea-ice model. No flux corrections are used, apart from a correction in the freshwater flux in the Arctic ocean to compensate excessive precipitation in this region. ECBilt is a factor 10–100 faster than more complex GCMs, so that it is possible to perform very long integrations.

The present-day mean climate is simulated reasonably well by ECBilt. The jet strength and the storm track are close to the observed state. There is a warm and wet bias in middle-to-high latitudes, especially in winter. In the tropics, variability is underestimated. In the extra-tropics, large-scale spatial patterns of variability compare favourably with observations (Selten *et al.*, 1999). ECBilt was applied earlier to the study of climatic variability in the late Holocene (Schrier *et al.*, 2002) as well as rapid transitions in the early Holocene (Renssen *et al.*, 2001).

Recently, a transient simulation of the Holocene climate was completed (Weber, 2001). The only forcing in this experiment is the change in insolation due to variations in the orbital parameters (Berger, 1978) for the period of 10 kyr BP (thousand years before present) up till now. The present-day control climate was used as the initial state. All other boundary conditions (orography, concentration of trace gases, surface characteristics) were set to their present-day values. The impact of relict ice sheets on the early-Holocene climate, CO_2 variations and feedbacks associated with changing vegetation patterns are thus not taken into account.

The glacier model

The glacier evolution is calculated with a flowline model. The model set-up is illustrated in Figure 1a. First, a flowline is selected along which the calculations are carried out. The parameterization of the three-dimensional geometry is done by prescribing the glacier width and slopes of the valley walls along the flowline. In this way, the width of the model glacier may vary in relation to the ice thickness. This is notably important when a glacier flows out in a gentle valley, gets wider and thereby increases the area of the ablation zone.

A prognostic equation for the evolution of the model glacier follows from integration of the continuity equation over glacier depth and width, yielding:

$$\frac{\partial S}{\partial t} = -\frac{\partial (US)}{\partial x} + wB \qquad (1)$$

Here x is distance along the flowline, t time, S the area of the cross-section perpendicular to the flowline, U the ice velocity along the flowline (averaged over S), $w = w_0 + \lambda H$ the width of the glacier at the surface as indicated in Figure 1a, and B the specific balance (averaged over the glacier width). The area S can easily be expressed in the parameters describing the shape of the valley. Substituting this expression in (1) then yields a rate equation for the ice thickness H. The analysis will not be given here, because it can be found elsewhere (Oerlemans, 1997).

The ice velocity U is entirely determined by the local 'driving stress' τ, being proportional to the ice thickness H and surface slope $\partial h/\partial x$ (h is surface elevation). There are two contributions to U: one from simple shearing flow (U_d) and one from sliding (U_s). The following expression is used (Budd *et al.*, 1979; Oerlemans, 1997):

$$U = U_d + U_s = f_d H \tau^3 + \frac{f_s \tau^3}{H} \qquad (2)$$

Although the sliding velocity depends on the water pressure, this is not explicitly dealt with. The bulk effect is supposed to be absorbed in the sliding parameter f_s. The values of f_d and f_s suggested by Budd *et al.* (1979), $f_d = 1.910^{-24}\ Pa^{-3}s^{-1}$ and $f_s = 5.710^{-20}\ Pa^{-3}m^2s^{-1}$, are used for all three glaciers. Substitution of (2) into (1) leads to the final prognostic equation for ice thickness H and thus for glacier length L (see Oerlemans, 1997).

The specific mass-balance of a glacier is determined by the annual-mean net effect per unit area of all processes that lead to a gain or loss of mass at the glacier surface, such as the absorbed short-wave radiation, net long-wave radiation, sensible and latent heat exchange, melting and (re-)freezing. In the context of the flowline model (1), we consider the specific balance averaged over the glacier width. It is assumed that B (in m/s) can be described as (Oerlemans, 1997):

$$B = B^{ref}(z) + \Delta B(t) + C \qquad (3)$$

Here B^{ref} is a reference profile, depending on the altitude z. It is independent of the definition of the flowline or the glacier geometry. The time-dependent mass-balance anomaly ΔB will be discussed in the next section. The constant C allows us to calibrate the mean glacier length over a given time period (e.g., the last 100 years of the simulation) to the present-day observed value. Measured mass-balance data show that annual mass-balance anomalies are indeed, to a first approximation, independent of altitude. Climatological-mean reference profiles B^{ref} are obtained from the World Glacier Monitoring Service (WGMS).

At a given distance x along the flowline, the altitude z is given by $h = b + H$, with b the bed elevation. The term B^{ref} in (3) thus

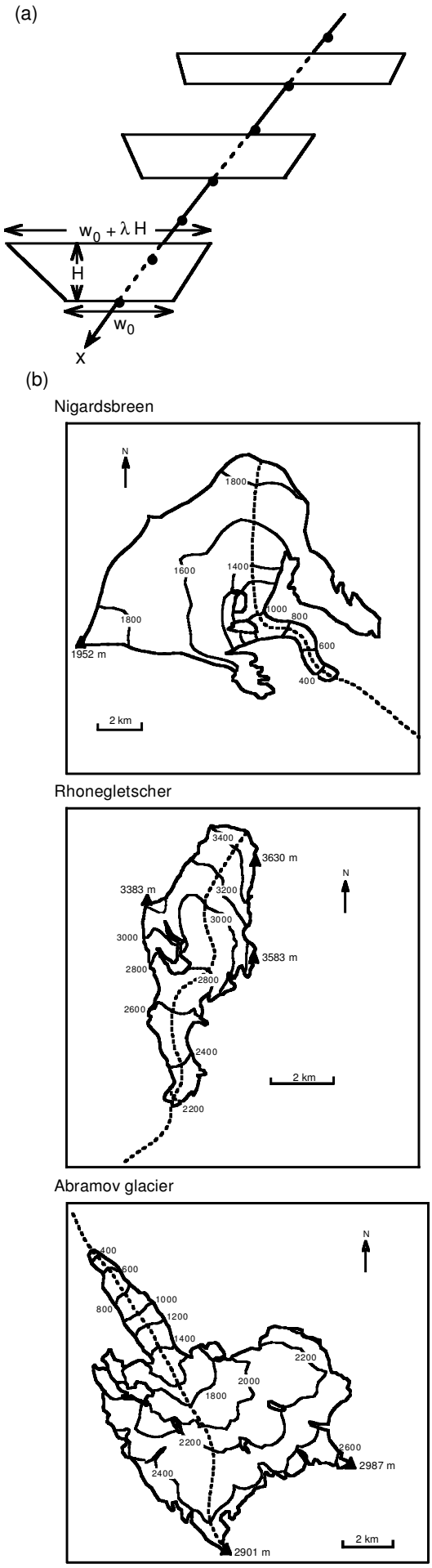

Figure 1 (a) Trapezoidal cross-section perpendicular to the flowline indicated by the x coordinate as used in the numerical glacier model. (b) Simple maps of the modelled glaciers. Dashed lines are the flowlines as defined for the numerical glacier model.

implicitly varies with time, because the ice thickness H at a given distance x varies with time. In general, the reference mass-balance increases with altitude. Therefore, this term contains the positive feedback of glacier surface elevation on the mass-balance.

The geometries of the glaciers studied here are shown in Figure 1b. It is clear that there are significant differences in the glacier geometries. The tongue of Nigardsbreen is very narrow compared to the accumulation basin, which makes its length (not volume) more sensitive to climatic change. Abramov glacier has a smoother shape and a smaller slope. Clearly, some ambiguity is involved in the choice of flowline. In the lower parts of the glacier it just follows the valley axis, but higher up it is not so clear which path to follow. Fortunately, the choice is not very critical to the model results as long as the area-elevation distribution is reproduced well.

Annual mass-balance anomalies

Anomalies in the specific mass-balance, averaged over the glacier area, can be obtained for a particular year from monthly surface air temperature and total precipitation anomalies using a Seasonal Sensitivity Characteristic (SSC; Oerlemans and Reichert, 2000). This gives the mean mass-balance anomaly with respect to a reference geometry as:

$$\Delta B_M = \sum_{i=1}^{12} (C_{i,T} T_i^A + C_{i,P} P_i^A) \tag{4}$$

Units are metres of water equivalent (mwe). The index i runs over the calendar months. The absolute anomaly in temperature T_i^A (in °C) and *relative* anomaly in precipitation P_i^A are defined as:

$$T_i^A = T_i - T_i^{ref} \text{ and } P_i^A = (P_i - P_i^{ref})/P_i^{ref} \tag{5}$$

where T_i^{ref}, P_i^{ref}, denote reference values of temperature and precipitation. The coefficients $C_{i,T}$, $C_{i,P}$, are the elements of the SSC. They characterize the glacier in terms of local meteorological conditions, such as the length of the melt season and the distribution of precipitation over snow and rain.

We now assume that the glacier-mean mass-balance anomaly ΔB_M can be used to compute the altitude-independent term $\Delta B(t)$ in (3):

$$\Delta B_M = 3.110^7 \, \Delta B \tag{6}$$

The factor 3.110^7 (the number of seconds in a year) relates ΔB (in m/s) to ΔB_M (in m or mwe). We use 100-year mean values of temperature and precipitation computed over the last century of the Holocene simulation as reference values in (5). Anomalies and reference values are taken at the grid-point nearest to the specific glacier location. As $\Delta B(t)$ does not depend on altitude, it can be applied to any geometry that is dynamically computed by the flowline model.

Some physical characteristics of Nigardsbreen, Rhonegletscher and Abramov glacier are given in Table 1. Glacier data can be obtained from the WGMS at its website (http://www.geo.unizh.ch/wgms) or through the five-yearly reports compiled by the WGMS on current changes in glaciers throughout the world (e.g., IAHS/UNESCO, 1998). The e-folding response time, given in Table 1, follows from imposing an instantaneous change in the climate forcing of the glacier model (Oerlemans, 2000).

The specific SSCs of the three glaciers are shown in Figure 2. Nigardsbreen is a maritime (wet climate) glacier, which extends to relatively low altitudes. Therefore, a significant fraction of precipitation falls as rain. This results in a large sensitivity to temperature (increased temperatures go with enhanced melt, but also with comparatively more rain). The temperature sensitivity is

Table 1 Glacier characteristics

Glacier	Nigardsbreen	Rhonegletscher	Abramov glacier
Area (in km^2)	48	18.5	25.9
Length (in km) at AD 1990	10.4	9.8	9.1
Altitudinal range (m)	300–2000	2100–3600	3600–5000
Response time (in yr)	68	58	92
$\sigma(\Delta B)$ (in mwe) *measured*	1.05	0.75	0.73
$\sigma(\Delta B)$ (in mwe) *simulated by ECBilt*	0.49	0.60	0.31

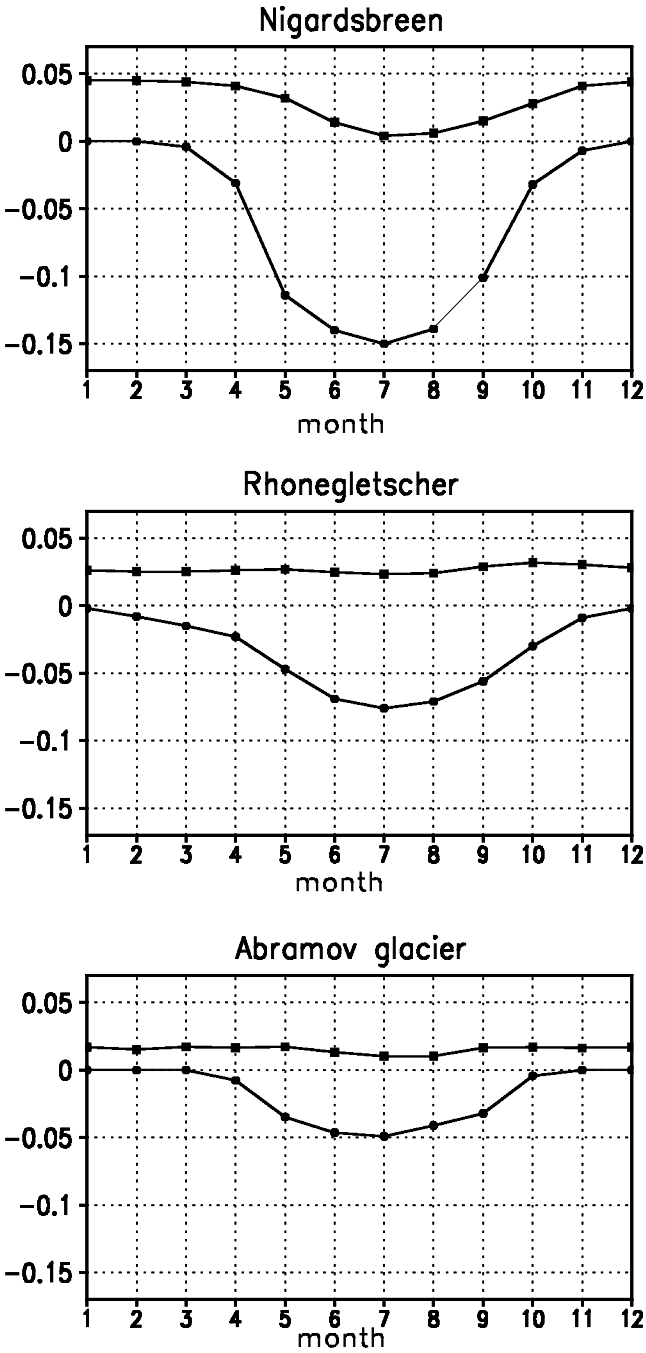

Figure 2 The seasonal sensitivity characteristic (SSC; see text) for Nigardsbreen, Rhonegletscher and Abramov glacier: temperature coefficients (in mwe/°C) of the SSC denoted by circles and precipitation coefficients (in mwe/(10%)) denoted by squares.

maximum in summer, while the melt season extends from April to October. The glacier sensitivity to precipitation is large in the cold season.

Rhonegletscher, located at higher altitudes, has a slightly more continental character. It is less sensitive to climatic conditions than Nigardsbreen, while the melt season has similar length. Precipitation changes affect the mass-balance throughout the year due to the higher elevation.

Abramov glacier is a continental (dry climate) glacier. It is again less sensitive than Rhonegletscher. The melt season is short, from May to June. Precipitation changes induce glacier growth or decay in all months of the year, with lowest sensitivity in summer.

Simulated glacier mass-balance variability

Now we will briefly discuss how realistic the simulated mass-balance variability is, comparing the climate of the last 100 years of the ECBilt simulation with NCEP/NCAR reanalysis data (Kalnay *et al.*, 1996). ECBilt underestimates the overall level of temperature variability, which is a common feature of coarse-resolution climate models. The seasonal pattern (larger variability in winter than in summer) is reasonably well simulated. The spatial pattern is too zonal, as the contrast between maritime and continental climates is not well captured. Compared to the reanalysis data, ECBilt overestimates temperature variability throughout the year for Nigardsbreen, while underestimating this for Abramov glacier. For Rhonegletscher, temperature variability is slightly underestimated.

Over Europe precipitation is generally most variable in months with a high mean precipitation. Variability in relative precipitation is thus comparatively independent of the time of the year. ECBilt captures this pattern fairly well for autumn-winter-spring. However, there is an unrealistic maximum in summer, especially for Rhonegletscher. The overall level of variability is again too low. For Abramov glacier, NCEP/NCAR variability in relative precipitation is maximum in July to October, when mean precipitation is very low. The timing of the maximum is well reproduced by ECBilt, although its amplitude is too small.

Monthly-mean temperature and precipitation anomalies result in anomalies in the annual mass-balance ΔB according to (4). The relative importance of temperature and precipitation during different times of the year is illustrated by the Seasonal Impact Characteristic (SIC), which combines the typical amplitude of climate anomalies with the glacier sensitivity to such an anomaly (Reichert *et al.*, 2001). The elements of the SIC are defined for each month as:

$$C_{i,T}\sigma_i(T) \quad and \quad C_{i,P}\sigma_i(P) \tag{7}$$

where $\sigma_i(T)$ and $\sigma_i(P)$ denote the standard deviation of monthly temperature and precipitation, respectively. The coefficients $C_{i,T}$ and $C_{i,P}$ are the elements of the SSC; compare equation (4). The SIC as simulated by ECBilt for the grid-point closest to the specific glacier site is given in Figure 3. The SIC computed from the NCEP/NCAR data for the corresponding location is shown as well in the figure.

It is clear that for Nigardsbreen the impact of (summer) temperature on the annual mass-balance is somewhat overestimated, while the impact of precipitation is underestimated during autumn-winter-spring. For Rhonegletscher, the simulated impact of (summer) temperature is approximately right. Compensating errors in the seasonal pattern of precipitation anomalies result in a reasonable amplitude of the annual-mean precipitation impact. For Abramov glacier, the impact of both temperature and precipitation is underestimated.

Measured values of the standard deviation of the annual mass-balance σ (ΔB) exist for Nigardsbreen and Abramov glacier. A value for Rhonegletscher can be estimated from measured data

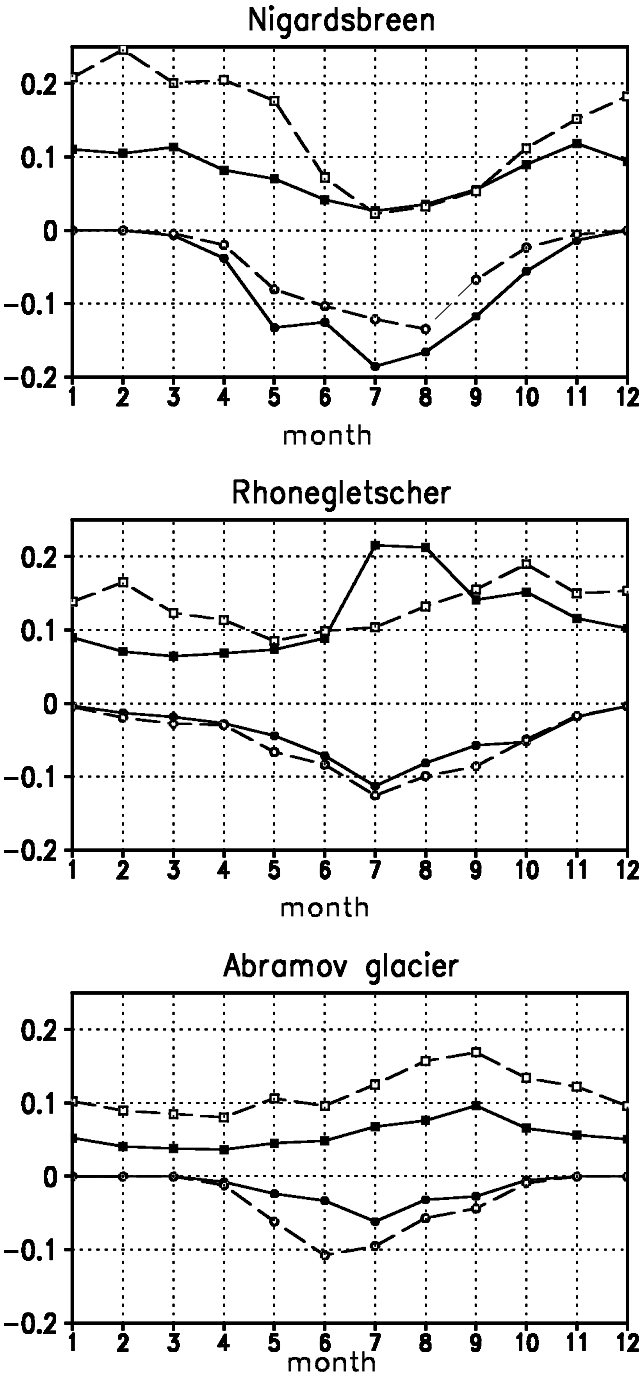

Figure 3 The seasonal impact characteristic (SIC; see text) for Nigardsbreen, Rhonegletscher and Abramov glacier: impact (in mwe) as simulated by ECBilt of interannual temperature anomalies (closed circles) and precipitation anomalies (closed squares). Also shown is the impact derived from NCEP/NCAR reanalysis data of temperature anomalies (open circles) and precipitation anomalies (open squares).

for the nearby Griesgletscher, which has a similar climate regime (Oerlemans, 2000). Measured data obtained from the WGMS and simulated data are given in Table 1 for the three glaciers. The value simulated by ECBilt is considerably too low for Nigardsbreen and Abramov glacier, while it is close to the estimated value for Rhonegletscher. Grid-point data give a reasonable estimate of the local climate, although variability is typically underestimated (Reichert *et al.*, 2001). The foregoing comparison to NCEP/NCAR data thus makes clear that mass-balance variability is simulated qualitatively correct by ECBilt. Only the seasonal pattern of precipitation variability for Rhonegletscher is not well captured, because ECBilt does not resolve the small-scale local orography.

The glacier model integrates the forcing over time. It is therefore of interest also to consider the SIC computed from the simulated low-pass filtered temperature and precipitation anomalies. As an example, we consider only timescales longer than 100 years. The low-pass filtered SIC was found to be very similar to the full SIC displayed in Figure 2, while its elements are smaller in amplitude by a factor of 10. This result is not unexpected, as the year-to-year autocorrelation of monthly data is small and the spectrum is (nearly) white. This aspect is clearly realistic. We therefore assume that the simulated low-pass filtered SIC has similar strengths and deficiencies to the full SIC discussed above. An interesting implication of the short atmospheric memory is that summer and winter are not significantly correlated. It follows that the simulated low-frequency variability is season-specific, a feature which has also been found in long instrumental records (Shabalova and Weber, 1998).

Climate model results

The early Holocene is characterized by a stronger insolation in boreal summer (June-July-August) as compared to present, especially at Northern Hemisphere middle-to-high latitudes. Insolation in boreal winter (December-January-February) was weaker, especially at low latitudes. This seasonal pattern persisted untill the late Holocene, while gradually becoming smaller in amplitude. As a result, Northern Hemisphere summers were generally warmer in the early Holocene as compared to today, especially over the continents at middle-to-high latitudes, and the African-Indian monsoon system was more intense. In winter, the subtropical land masses were cooler than today.

We first consider the spatial response pattern for the period 6 kyr BP and try to assess how realistic the present simulation is. Focus is on the western/central Eurasian region (20–80°N, 20°W–90°E), where the three glaciers are located. Next we describe the long-term temporal evolution at the three glacier locations.

The mid-Holocene Optimum

The mid-Holocene Optimum is one of the focal periods of the Paleoclimate Modeling Intercomparison Project (PMIP) (Joussaume *et al.*, 1999). Within the framework of PMIP, extensive data syntheses have been undertaken and a large number of (atmosphere-only) model simulations have been performed. Therefore, the response patterns obtained at 6 kyr BP in the present simulation can be compared to proxy-based evidence as well as earlier model results for this period.

Over Europe climate reconstructions based on pollen and lake-level data (Cheddadi *et al.*, 1997) indicate a wintertime warming over northeastern Europe and a cooling over southern Europe, with no significant changes over central and northwestern Europe. Reconstructed summer temperatures were higher than at present in the mountainous regions of Scandinavia, Great Britain and the Alps, whereas they were lower in southern Europe and there were no significant changes elsewhere. At both glacier locations, proxy data indicate a direct temperature response to the insolation forcing (insignificant change in winter, warming in summer), which is simulated qualitatively well by ECBilt. The response in July temperature is shown in Figure 4. Other features are not so well captured, in agreement with earlier PMIP modelling results. Models tend to simulate the direct response to the insolation forcing correctly, but vary widely in the simulated location and intensity of any indirect response (Masson *et al.*, 1999).

Quantitative reconstructions indicate that July temperatures were warmer than today by about 2°C in southern Scandinavia and by about 4°C at high altitudes in central Europe (Huntley and Prentice, 1988), although the latter figure may be overestimated

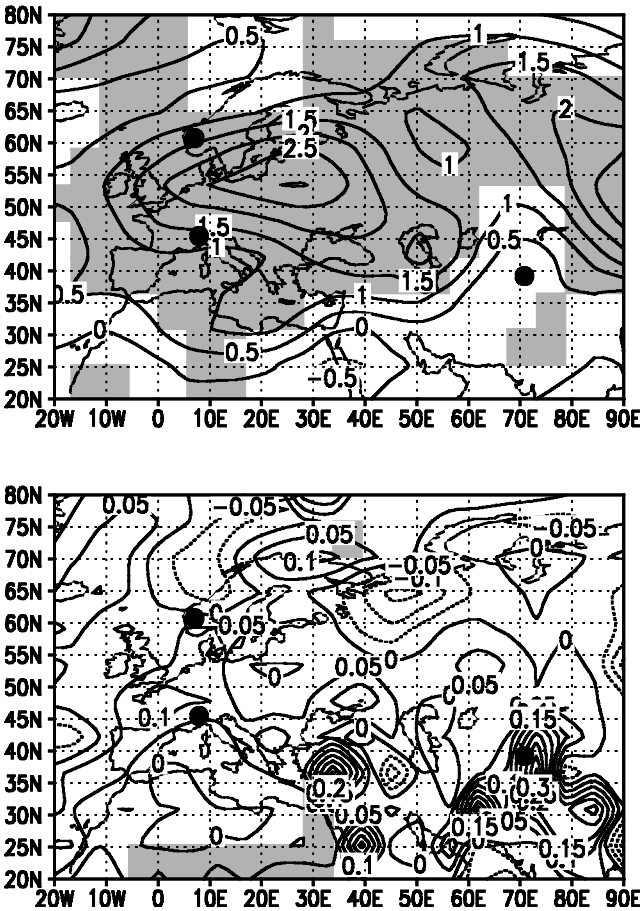

Figure 4 The response in July temperature (in °C; upper panel) and in the annual water budget (in mm/day; lower panel) to the orbital forcing at 6 kyr BP as simulated by ECBilt for the west/central Eurasian region. Shown is the 100-year mean anomaly with respect to the last 100 years of the Holocene experiment. Shading indicates significance at the 95% level, derived from a local two-sided t-test. Glacier locations are indicated by dots.

(Cheddadi *et al.*, 1997). ECBilt simulates a similar (Nigardsbreen) or somewhat lower figure (Rhonegletscher).

Southern and eastern Europe seem to have been wetter, whereas the regions of reconstructed summer warming were dryer than today for the mid-Holocene climate (Cheddadi *et al.*, 1997). Earlier model experiments are not conclusive with respect to the precipitation response (Yu and Harrison, 1996; Masson *et al.*, 1999). In ECBilt changes in the annual water budget (precipitation minus evaporation) are smaller than 0.1 mm/day everywhere over Europe, as shown in Figure 4 (lower panel). This is statistically not significant.

Over the continental interior of Eurasia summer temperatures are thought to increase in response to the insolation forcing, which causes the amplification of the African-Indian monsoon (Joussaume *et al.*, 1999). Lake data indicate conditions similar to or wetter than today over the continental interior of Eurasia, which is hypothesized to be due to a northward shift of the summer monsoon precipitation into Eurasian mid-latitudes up to 50N (Yu and Harrison, 1996). ECBilt simulates warmer summers over central Eurasia, with a wetter climate at latitudes 20–40°N. Changes in the water budget are due to increased summer monsoon precipitation in a belt extending from the Arabian peninsula to Kazakhstan. They are statistically significant in the months of maximum response only. Such a northward expansion of the Asian monsoon has been found in a number of PMIP simulations as well, although its magnitude and extent seem to be underestimated as compared to lake data (Yu and Harrison, 1996). The increased amount of surface water results in enhanced evaporation and thus in a lower surface temperature response in this region than one would expect from the insolation forcing alone.

Summarizing, we can conclude that the temperature response at the two European glacier sites is reasonably well simulated by ECBilt, although the actual response at Rhonegletscher may have been stronger. It is impossible to assess seasonal precipitation changes, as proxy data representing the annual water budget are not conclusive and models differ widely among each other. The wetter climate at Abramov glacier seems to be supported by data and some earlier model results. A relatively small summer temperature response here is consistent with an enhanced hydrological cycle. Quantitative estimates of water-budget changes for this region do not exist.

Long-term evolution

The insolation forcing at mid-latitudes is shown in Figure 5 for JJA and for the individual months of the warm season. The temporal pattern is similar for each glacier site, as the meridional gradient is small at mid-latitudes. Summer insolation peaks in the early Holocene. However, the monthly insolation maximum migrates first from June to July (around 8.5 kyr BP) and then to August (around 4 kyr BP). The direct temperature response to the Holocene insolation changes is thought to follow the forcing quasi-linearly (Crowley and North, 1991).

Dahl and Nesje (1996) give an estimate for southern Norway of the Holocene evolution of summer temperature, based on subfossil pines, and winter precipitation. The latter is obtained by combining summer temperatures with reconstructed equilibrium-line altitude fluctuations of Hardangerjøkulen. The long-term climate trend indeed consists of a gradual change. Summer temperatures were warmer by at least 1.2–1.4°C and winter precipitation was higher by 50% at 10–9 kyr BP (Dahl and Nesje, 1996). This gradual-change pattern is interrupted by several periods lasting a few hundred years, which are characterized by cold summers and dry winters. The first and largest of these 'events' is synchronous with the relatively cold episode around 8.2 kyr BP identified in Greenland ice cores (Johnsen *et al.*, 1992).

The temporal pattern of change in lake-status data is described by Harrison *et al.* (1996). They also describe a gradual change in Europe after the retreat of the Scandinavian ice sheet (around 9 kyr BP). In contrast to this, the Asian monsoon intensifies during the early Holocene to reach its maximum around 6–5 kyr BP. Then there is a gradual transition to modern conditions. The monsoon response is found to lag the JJA insolation forcing by a few thousand years.

Now the response of the local climate at each glacier location, as simulated by ECBilt, will be discussed in more detail. As we

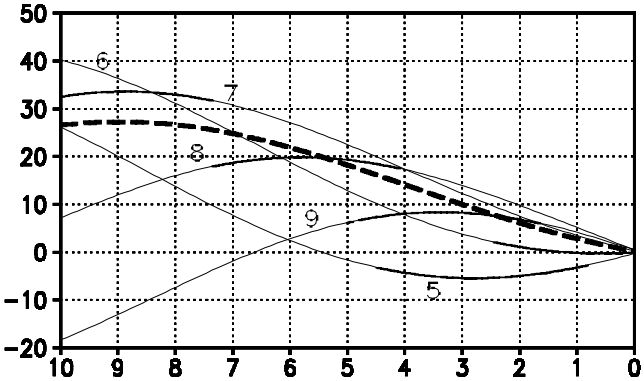

Figure 5 The insolation forcing (in W/m^2) due to changes in the Earth's orbit as a function of time (in kyr before present) for the latitudinal belt 40–60°N. Shown are consecutive 100-year mean anomalies with respect to the last 100 years of the Holocene experiment for June-July-August (thick dashed line) and for the months May (5), June (6), July (7), August (8) and September (9).

are primarily interested in the impact of climate anomalies on the glaciers, we consider the contribution of monthly temperature and precipitation anomalies to the annual mass-balance anomaly rather than the climate anomalies themselves. The monthly contributions are given by the terms on the right-hand side of equation (4):

$$C_{i,T}T_i^A \quad and \quad C_{i,P}P_i^A \tag{8}$$

In order to focus on the orbitally forced trend, variability on interannual to centennial timescales is filtered out by taking the 999-year running mean.

The results for Nigardsbreen are shown in Figure 6a. The impact ΔB_T of temperature anomalies on the mass-balance is clearly much larger than the impact ΔB_P of precipitation anomalies, while the two terms have opposite sign. July and August temperatures, which are about 3°C higher at 9 kyr BP than they are today, are mainly responsible for the negative anomaly in ΔB_T. There is a smaller contribution from June and September. The temperature response lags the insolation forcing by one month, due to the thermal inertia of the nearby ocean. Winter precipitation is 10% higher than today, which is associated with a slightly deeper Icelandic Low and stronger westerly flow. The amplitude of this signal is small, but it is consistently present throughout the cold season (November to April). This results in a small positive anomaly in ΔB_P. The combined effect of temperature and precipitation results in a negative mass-balance at Nigardsbreen in the early Holocene, which gradually decays in time.

Rhonegletscher (Figure 6b), is less sensitive to temperature anomalies than Nigardsbreen. The temperature impact on the glacier mass-balance is therefore smaller here, although the temperature anomalies themselves have similar amplitude. The negative anomaly in ΔB_T is mainly determined by the month July, with smaller contributions from August and June. At this more inland location, the response lags the forcing by less than a month. Summer precipitation over central Europe is stronger than today, due to local monsoon-type circulations. As summer evaporation increases as well, this has a negligible effect on the annual water budget. However, the relative change is considerable (40–50%). This results in a positive anomaly in ΔB_P, which persists until 3–4 kyr BP. The total mass-balance shows a small negative anomaly until about 6 kyr BP, when ΔB_T and ΔB_P balance. After that, there is a small positive anomaly which only disappears in the late Holocene.

The long-term impact on the mass-balance of Abramov glacier is shown in Figure 6c. The largest climate signal is seen in summer precipitation, which is stronger than today from June to September. The relative change is especially large late in the rainy season, when the absolute amount of rainfall in the present-day climate is small. Therefore, there is a significant contribution to ΔB_P in July and August in the early Holocene. The contribution to ΔB_P of September rainfall peaks at about 6 kyr BP, in response to the increasing August insolation. The combined effect causes a maximum anomaly in ΔB_P at 6 kyr BP and a gradual decrease afterwards. Temperature anomalies are relatively small at Abramov glacier. Consequently, ΔB_T shows a small and gradually decaying negative anomaly. The total mass-balance shows an increasing positive anomaly until about 6 kyr BP. From the mid-Holocene onward, ΔB decreases until it is zero at about 3 kyr BP.

The temporal pattern of change in ΔB_T at Nigardsbreen and Rhonegletscher seems realistic. It is a direct, lagged response to the monthly insolation forcing. At Nigardsbreen, the amplitude of the simulated temperature signal is higher than the estimate of Dahl and Nesje (1996), but it is close to the figure given by Huntley and Prentice (1988) for 6 kyr BP. At Rhonegletscher, the simulated amplitude may be too low. Proxy data indicate that winters were considerably wetter at Nigardsbreen in the early Holocene compared to present. ECBilt does simulate a small but persistent increase in relative winter precipitation, albeit of a much smaller amplitude than proposed by Dahl and Nesje (1996). At Rhonegletscher, ECBilt simulates higher summer precipitation in the early Holocene. It is not clear whether this signal is realistic, but it has a large impact on the simulated evolution of ΔB. At Abramov glacier, the temporal pattern in ΔB_P, as inferred from proxy data (Harrison *et al.*, 1996), seems well captured by ECBilt. The evolution of ΔB_T is consistent with stronger summer insolation, combined with high evaporation levels. It seems likely that the amplitude of the precipitation signal is underestimated by ECBilt, as there is no significant change in the simulated annual water budget.

Glacier changes in response to climate forcing

The glacier ice-flow model computes a 10 kyr record of glacier length for each glacier, given the annual mass-balance ΔB computed from the climate model output. It takes several hundreds of years before the initial glacier length, which was set to zero, has adjusted to the forcing. Results are shown for Nigardsbreen, Rhonegletscher and Abramov glacier in Figure 7. The long-term trends in glacier length, as given by the 999-year running mean values, are shown as well. The trends clearly reflect the orbitally forced signal in ΔB discussed earlier.

At Nigardsbreen, the glacier length slowly increases at first; then there is a period of rapid expansion, followed by more gradual growth. The long-term trend primarily reflects the July and August temperature response to orbital forcing. Rhonegletscher gradually increases in length until a levelling-off around 5 kyr BP, followed by a small decrease in the last two millennia of the experiment. At first, the glacier length is determined by the combined effect of the temperature and precipitation response, mainly in July and August. After that, ΔB_T is close to zero and the trend results solely from the long-term signal in ΔB_P. At Abramov glacier, the length shows the smallest changes during the Holocene experiment. There is a small increase until about 6 kyr BP, followed by a decrease during the next 3 kyr. High summer precipitation, which peaks at the mid-Holocene, is only partly compensated by warmer summer temperatures. This results in the maximum extent at 6 kyr BP and the gradual decrease after that.

The variability on timescales shorter than millennial, which is evident in Figure 7, is related to internally generated variability of the climate parameters forcing the glacier model. It is clear from Figure 7 that for Nigardsbreen the standard deviation in glacier length $\sigma(L)$ depends on time, varying from 0.15 km during the first millennia to 0.7 km directly afterwards and 0.4 km for the present-day climate. This is primarily due to variations in glacier sensitivity, as $\sigma(\Delta B)$ does not change much during the Holocene. The sensitivity of glacier length to mass-balance changes depends on the specific length range: Nigardsbreen exhibits a rapid expansion as well as large variability in the length range 5–10 km. This is related to the geometry of the area occupied by the glacier snout. In the sensitive length range, the glacier snout passes through a narrow valley. At Rhonegletscher and Abramov glacier, the simulated lengths fall in a small range of values, so that this effect is not visible.

Glacier length spectra are shown in Figure 8. Although ΔB shows variability on all timescales, there is no power in the length spectrum for timescales shorter than about 50 years (Rhonegletscher), 80 years (Nigardsbreen) and 100 years (Abramov glacier). Clearly, the glacier length constitutes an integrated response to the simulated mass-balance changes. The mass-balance spectra are white for timescales longer than 5–10 years. In contrast to this, the glacier length spectra have maximum power at timescales 300–400 years (Rhonegletscher), about 500 years

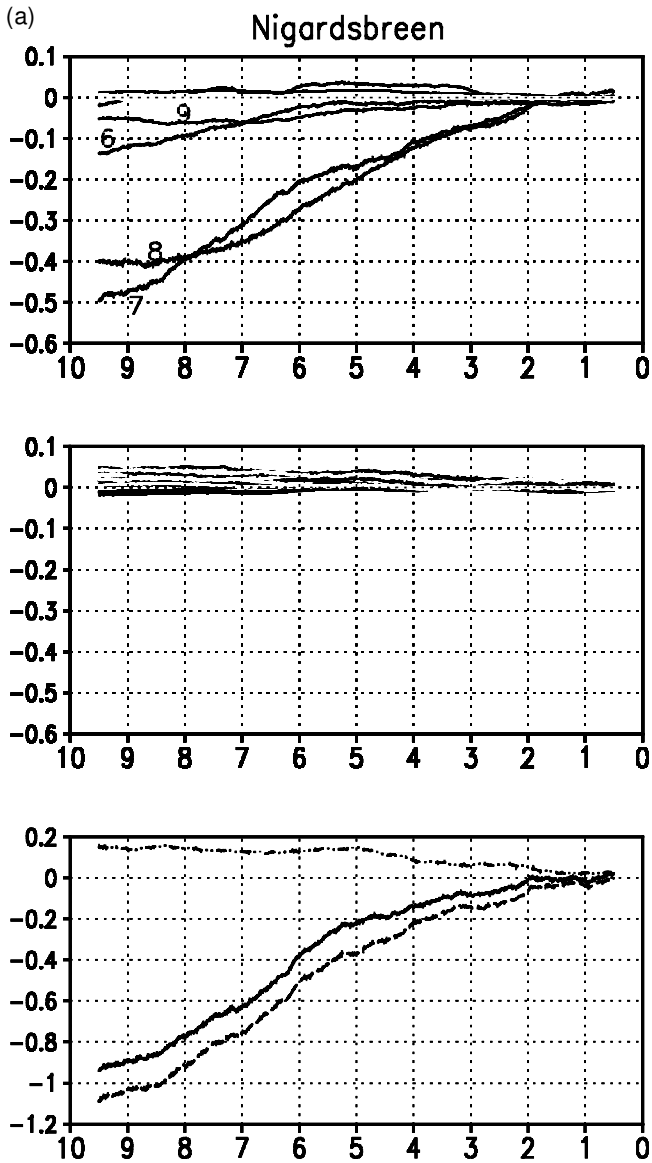

Figure 6 The impact as simulated by ECBilt of long-term monthly temperature anomalies (upper panel) and precipitation anomalies (middle panel) on the annual-mean mass-balance of (a) Nigardsbreen, (b) Rhonegletscher and (c) Abramov glacier as a function of time (in kyr before present). The impact is defined in the text. The lower panel gives the total temperature contribution ΔB^T (dashed) and precipitation contribution ΔB^P (dot-dashed) to the long-term annual mass-balance ΔB (solid line) (all units: mwe).

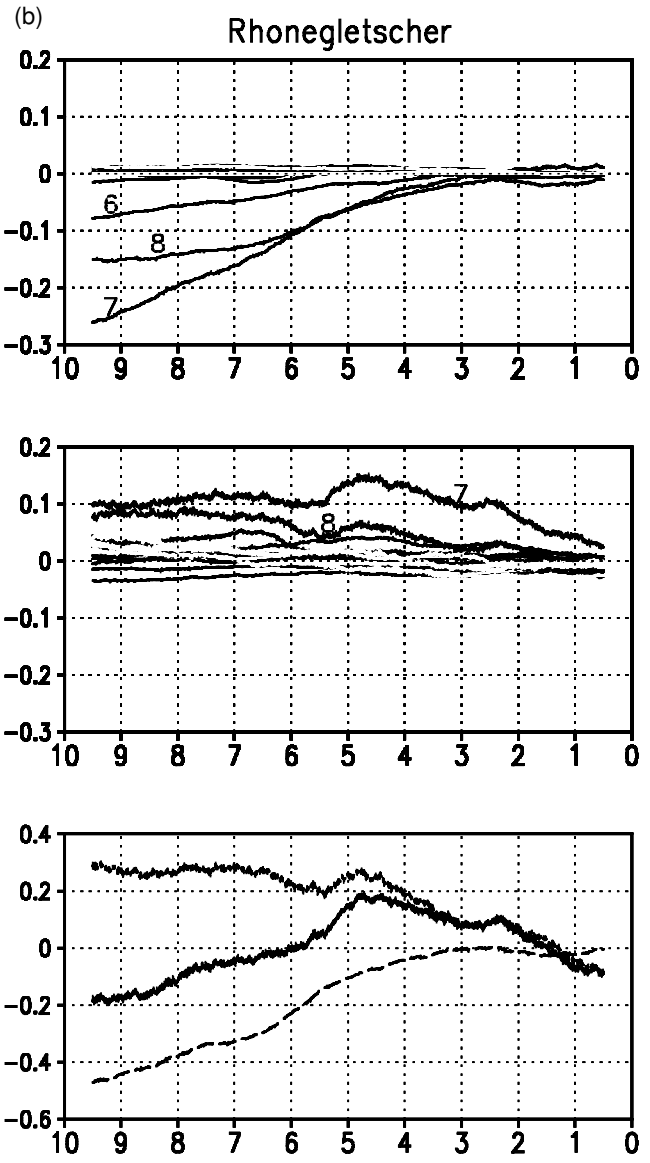

Figure 6 Continued.

(Nigardsbreen) and even longer (Abramov glacier). There are no significant periodicities.

In order to examine the relation between forcing ΔB and length L in more detail, a moving average (MA) process of order q (Von Storch and Zwiers, 1999) was used to fit the data:

$$L_{n+m} = \frac{\beta}{q+1} \sum_{j=0}^{q} \Delta B_{n-j} \qquad (9)$$

Here the index n loops over time (in years). The right-hand side contains the mean forcing over the previous $(q + 1)$ years, with β the regression coefficient (in km/mwe). The memory of such a process is q years. The response on the left-hand side lags the forcing by m years. Various low-pass filters ($q = 50, 80, 100, 150$) were applied to the detrended mass-balance record. Optimal fits were obtained with a lag of 10–20 years. For Rhonegletscher, the maximum correlation is $\rho = 0.91$ with a memory $q = 50$ ($\beta = 2.2$ km/mwe) and for Abramov glacier this is $\rho = 0.93$ with $q = 100$ ($\beta = 3.7$ km/mwe). For Nigardsbreen, $\rho = 0.89$ with $q = 80$ ($\beta = 7.6$ km/mwe), using the segment 7–0 kyr BP only. The memory of this glacier is found to be smaller in the first millennia of the Holocene. Therefore, use of the entire record results in a worse fit ($\rho = 0.76$).

The glacier length can thus be described as a lagged MA(q) process. The lag is determined by the rate of ice flow from the accumulation area of the glacier to the ablation area. The memory of each glacier is consistent with the cut-off points for the high-freqency part of the specific spectra. The pattern of increasing timescale for Rhonegletscher, Nigardsbreen and Abramov glacier agrees with the specific response times given in Table 1.

The relation (9) can be understood as follows. Fluctuations in glacier length (ice volume) are due to the time-dependent mass-balance forcing ΔB, to the feedback of ice thickness on the mass-balance through the altitude-dependent part of the forcing, and to changes in the glacier area and associated mass-balance effects. The second term is, to a first approximation, proportional to the change in glacier thickness, which is again proportional to the change in glacier length. Changes in glaciated area can also be assumed to be proportional to glacier length. On the timescales considered here, the forcing terms (almost) balance. For this reason, glacier length fluctuations are proportional to ΔB. The pro-

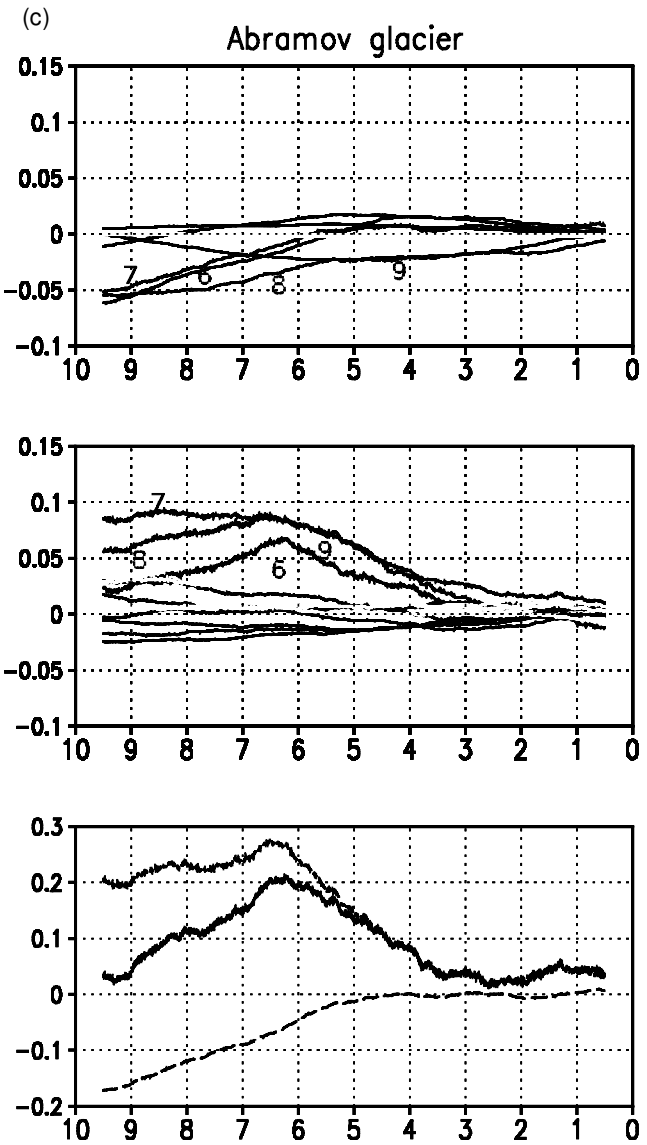

Figure 6 Continued.

portionality factor β depends on glacier characteristics like the thickness/length ratio and the gradient in the reference mass-balance profile.

The standard deviation in glacier length, computed over the entire 10 kyr record, is 0.42 km for Nigardsbreen, 0.26 km for Rhonegletscher and 0.17 km for Abramov glacier. It seems reasonable to conclude from (9) that length variations are simulated by ECBilt with the same accuracy as mass-balance variations. Measured and simulated values of $\sigma(\Delta B)$ are given in Table 1. They show that the standard deviation in mass-balance is underestimated at Nigardsbreen and Abramov glacier by (more than) a factor of 2, while it is approximately correct at Rhonegletscher. This indicates a similar skill for the simulated $\sigma(L)$. We can also compare the present figures with those obtained by Oerlemans (2000), who used random forcing of a realistic strength to drive the glacier model. He found standard deviations of 0.61 km for Nigardsbreen and 0.24 km for Rhonegletscher. This confirms that ECBilt underestimates $\sigma(L)$ at Nigardsbreen by about a factor of 2, but comes close to a realistic value at Rhonegletscher.

Estimates of $\sigma(L)$ thus range from a few hundred metres to almost one kilometre. Given the considerable amplitude of glacier length variations, we hypothesize that the smaller 'events' identified by Dahl and Nesje (1996) for Hardangerjøkulen (central south Norway) are manifestations of internal variability of the local climate rather than externally forced.

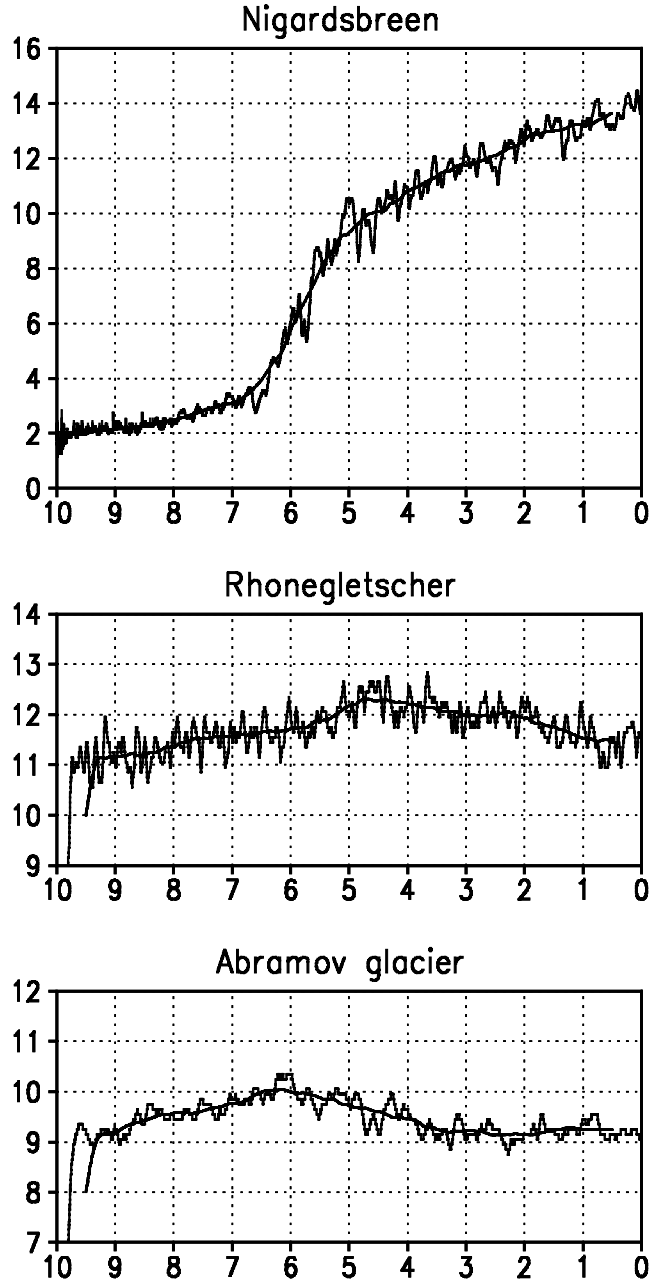

Figure 7 The glacier length (in km) as simulated by ECBilt for the three glaciers Nigardsbreen, Rhonegletscher and Abramov glacier as a function of time (in kyr before present). The long-term trends, as given by the 999-year running mean, are also shown.

Low-frequency variability in ΔB at Nigardsbreen is mainly determined by temperature anomalies. However, precipitation anomalies cannot be neglected. The two components are negatively correlated ($\rho = -0.27$ for the low-pass filtered data). The correlation is very weak, but it is consistent in consecutive millennia. It results from a positive correlation between temperature and precipitation anomalies throughout the cold season (November to March). At Nigardsbreen, variability in glacier length is thus mainly related to centennial-timescale variations in ΔB_T, with a smaller contribution from variations in ΔB_P. There is a weak tendency for the latter to counteract the former. However, in many cases variations in ΔB_T and ΔB_P randomly reinforce or weaken each other.

At Rhonegletscher, variability in glacier length is dominated by centennial-timescale variations in ΔB_P. At Abramov glacier, the two components of ΔB are positively correlated ($\rho = 0.67$ for the low-pass filtered data). This is due to a negative correlation between temperature and precipitation anomalies in summer (June

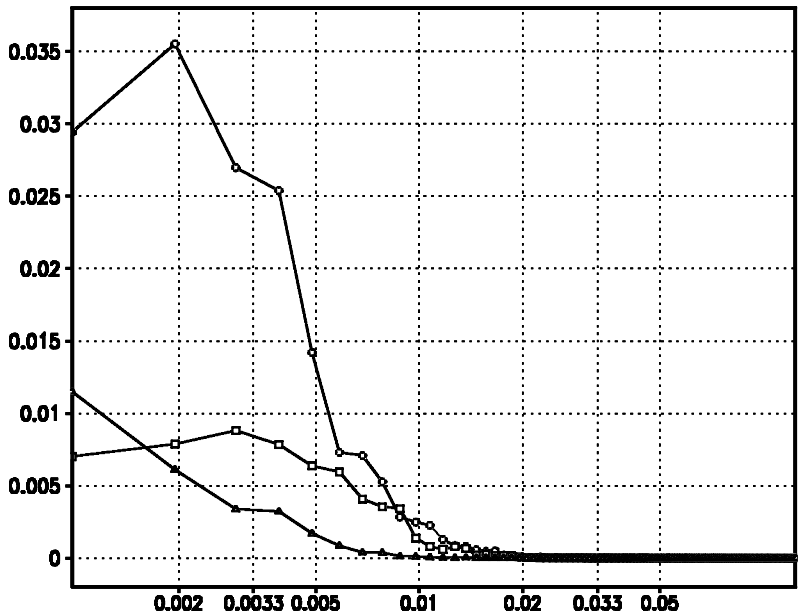

Figure 8 Length spectra (in km^2) for the three glaciers Nigardsbreen (circles), Rhonegletscher (squares) and Abramov glacier (triangles), computed from the detrended records. Frequency is given in cycles/year.

to August), which is typical for a monsoon climate. Variations in ΔB_T tend to reinforce variations in ΔB_P, while the former are smaller than the latter by about a factor of 3. Length variations of Abramov glacier are thus determined by both components.

Summary and conclusions

Synthetic glacier length records have been generated by a glacier model coupled to an intermediate-complexity climate model. The glacier model consists of a dynamic ice-flow component and a component which converts monthly temperature and precipitation anomalies to annual mass-balance anomalies. The climate model ECBilt has been run for 10 kyr. The only forcing in this transient experiment is the insolation change due to variations in the Earth's orbital parameters during the Holocene. Other external forcings, like solar irradiance changes, volcanic activity or anthropogenic effects, are not taken into account. Temperature and precipitation anomalies arise as a result of both the long-term orbital forcing and internally generated variability. We consider three glaciers, ranging from maritime to continental. They are Nigardsbreen in southern Norway, Rhonegletscher in the Swiss Alps and Abramov glacier in Kirghizia.

For Nigardsbreen and Rhonegletscher, proxy data indicate a direct temperature response (no significant change in winter and warming in summer) to the insolation forcing of the early Holocene (Cheddadi *et al.*, 1997). The annual water budget (precipitation minus evaporation) seems to have been reduced in regions where summers were warmer than today, but the seasonality of the signal or its distribution over precipitation and evaporation cannot be unambiguously determined. Additional proxy-based evidence (Dahl and Nesje, 1996) points to higher winter precipitation in the early Holocene for southern Norway.

At Nigardsbreen, the simulated glacier length shows a phase of rapid, strong expansion followed by more gradual growth. The postglacial maximum is reached for the present-day climate, as summer temperatures and winter precipitation decreased during the last 10 kyr. The negative mass-balance anomaly in the early Holocene is primarily determined by the summer temperature signal, with a smaller contribution from the winter precipitation signal. Both signals are consistent with data. The simulated amplitude of the winter precipitation signal is small compared to the quantitative estimate given by Dahl and Nesje (1996). However, a larger signal in winter precipitation would imply a length range very similar to today's for the entire Holocene. This does not seem likely. We therefore hypothesize that winter precipitation was increased in the early Holocene by a smaller amount than proposed by Dahl and Nesje (1996).

Rhonegletscher reaches its postglacial maximum during the mid- to late Holocene in the ECBilt simulation. After that, the glacier snout recedes on average a few hundred metres. The simulated long-term trend, which is due to decreasing summer temperature and precipitation, does not seem realistic. The summer temperature signal is consistent with the data. Therefore, we conclude that the summer precipitation response to the insolation forcing (higher in the early Holocene than today) is not realistic.

Proxy data indicate warmer summers over the Asian continent and a more intense Asian summer monsoon, which extended much further north than today (Joussaume *et al.*, 1999). Higher lake levels as far north as 50°N are hypothesized to be due to stronger monsoon precipitation (Harrison *et al.*, 1996). Maximum lake levels occurred around 6 kyr BP.

Abramov glacier reaches a pronounced postglacial maximum at 6 kyr BP in the ECBilt simulation. The maximum extent is on average 1 km longer than the present-day value. Mass-balance anomalies are mainly determined by June to September precipitation, which increases until about 6 kyr BP and then decreases to its present-day value. The precipitation response lags the insolation forcing by one month. The timing of the maximum, which is consistent with the lake-level data, follows directly from the monthly insolation maxima. Summer temperatures gradually decrease during the Holocene at Abramov glacier, which slightly offsets the precipitation effect.

The implication of the monsoon region extending this far north in the early Holocene is clearly illustrated by the present experiment. If this hypothesis is true, then there has been a considerable glacial advance in this region during the mid-Holocene and glacial retreat after that. This should be recognizable in the field by the remains of end-moraines. It is likely that ECBilt underestimates the amplitude of the precipitation signal, as there is no significant change in the simulated annual water budget. A larger precipitation signal (and the associated smaller temperature signal) would result in an even larger glacial advance.

There is considerable variability on timescales shorter than

millennial in the simulated glacier length records. These length variations are generated by internal variability of the climatic parameters forcing the glacier model. ECBilt has reasonable skill in simulating the relative importance of temperature and precipitation as well as the seasonality of the forcing. However, the overall level of variability is underestimated. Length variations can be described as a lagged moving-average process. Such a process integrates the (mass-balance) forcing over time. The lag is found to be 10–20 years. The glacier memory ranges from 50 years (Rhonegletscher) and 80 years (Nigardsbreen) to 100 years (Abramov glacier), consistent with the respective response times. There is maximum spectral power on centennial timescales, while the maximum shifts to lower frequencies as the memory of the glacier system increases.

At Nigardsbreen, simulated glacier length variations are determined by variability in summer temperature and in winter precipitation. In general, variations in ΔB_T and ΔB_P randomly reinforce or weaken each other. At Rhonegletscher, glacier length variability is primarily related to variability in precipitation throughout the year. At Abramov, length variations depend on both components, while variations in ΔB_T tend to reinforce variations in ΔB_P. Glacier length variations are typically asynchronous among the three different glaciers. Centennial-timescale variations in glacier length are found to have similar amplitude as the orbitally forced trend, except in the length range where the glacier sensitivity is very high. The present study illustrates the importance of Holocene glacier length variability on suborbital timescales. Internal climatic variability alone can explain such length variations.

References

Berger, A. 1978: Long-term variations of daily insolation and Quaternary climatic changes. *Journal of Atmospheric Science* 35, 2362–67.

Budd, W.F., Keage, P.L. and **Blundy, N.A.** 1979: Empirical studies of ice sliding. *Journal of Glaciology* 23, 157–70.

Cheddadi, R., Yu, G., Guiot, J., Harrison S.P. and **Prentice, I.C.** 1997: The climate of Europe 6000 years ago. *Climate Dynamics* 13, 1–9.

Crowley, T.J. and **North, G.R.** 1991: *Paleoclimatology.* New York: Oxford University Press, 349 pp.

Dahl, S.O. and **Nesje, A.** 1996: A new approach to calculating Holocene winter precipitation by combining glacier ELA and pine-tree limits: a case study from Hardangerjøkulen, central south Norway. *The Holocene* 6, 381–98.

Harrison, S.P., Yu, G. and **Tarasov, P.E.** 1996: Late Quaternary lake-level record from northern Eurasia. *Quaternary Research* 45, 138–59.

Huntley, B. and **Prentice, I.C.** 1988: July temperatures in Europe from pollen data, 6000 years before present. *Science* 241, 687–90.

IAHS/UNESCO 1998: *Fluctuations of glaciers 1990–1995. Volume VII.* Zurich: World Glacier Monitoring Service, 312 pp.

Johnsen, S.J., Clausen, H.B., Dansgaard, W., Fuhrer, K., Gundestrup, N., Hammer, C.U., Iversen, P., Jouzel, J., Stauffer, B. and **Steffensen, J.P.** 1992: Irregular glacial interstadials recorded in a new Greenland ice core. *Nature* 359, 311–13.

Joussaume, S., and **33 co-authors** 1999: Monsoon changes for 6000 years ago: results of 18 simulations from PMIP. *Geophysical Research Letters* 26, 859–62.

Kalnay, E., Kanamitsu, M., Kistler, R., Collins, W., Deaven, D., Gandin, L., Iredell, M., Saha, S., White, G., Woollen, J., Zhu, Y., Chelliah, M., Ebisuzaki, W., Higgens, W., Janowiak, J. Mo, K.C., Ropeliwski, C., Wang, J., Leetmaa, A., Reynolds, R., Jenne, R. and **Joesph, D.** 1996: The NCEP/NCAR 40-year reanalysis project. *Bulletin of the American Meteorological Society* 77(3), 437–71.

Masson, V., Cheddadi, R., Braconnot, P., Joussaume, S. and **PMIP participants** 1999: Mid-Holocene climate in Europe: what can we infer from PMIP model-data comparisons? *Climate Dynamics* 15, 163–82.

Oerlemans, J. 1997: A flow-line model for Nigardsbreen: projection of future glacier length based on dynamic calibration with the historic record. *Annals of Glaciology* 24, 382–89.

——— 2000: Holocene glacier fluctuations: is the current rate of retreat exceptional? *Annals of Glaciology* 31, 39–44.

Oerlemans, J., and **Reichert, B.K.** 2000: Relating glacier mass balance to meteorological data using a seasonal sensitivity characteristic (SSC). *Journal of Glaciology* 46(152), 1–6.

Opsteegh, J.D., Haarsma, R.J., Selten, F.M. and **Kattenberg, A.** 1998: ECBilt: a dynamic alternative to mixed boundary conditions in ocean models. *Tellus* 50A, 348–67.

Reichert, B.K., Bengtsson, L. and **Oerlemans, J.** 2001: Midlatitude forcing mechanisms for glacier mass balance investigated using general circulation models. *Journal of Climate* 14, 3767–84.

——— 2002: Recent glacier retreat exceeds internal variability. *Journal of Climate* 15, 3069–81.

Renssen, H., Goosse, H., Fichefet, T. and **Campin, J.M.** 2001: The 8.2 kyr event simulated by a global atmosphere/sea-ice/ocean model. *Geophysical Research Letters* 28, 1567–70.

Schrier, G. van der, Weber, S.L. and **Drijfhout, S.S.** 2002: Sea level changes in the North Atlantic by solar forcing and internal variability. *Climate Dynamics* 19, 435–47.

Selten, F.M., Haarsma, R.J. and **Opsteegh, J.D.** 1999: On the mechanism of North Atlantic decadal variability. *Journal of Climate* 12, 1956–73.

Shabalova, M.V. and **Weber, S.L.** 1998: Seasonality of low-frequency variability in early-instrumental temperatures. *Geophysical Research Letters* 25, 3859–62.

Von Storch, H. and **Zwiers, F.** 1999: *Statistical analysis in climate research.* Cambridge: Cambridge University Press, 484 pp.

Weber, S.L. 2001: The impact of orbital forcing on the climate of an intermediate-complexity coupled model. *Global and Planetary Change* 30, 7–12.

Yu, G. and **Harrison, S.P.** 1996: An evaluation of simulated water balance of Eurasia and northern Africa at 6000 y BP using lake status data. *Climate Dynamics* 12, 723–35.